RSC Advances

PAPER

View Article Online
View Journal | View Issue

Cite this: *RSC Adv.*, 2025, **15**, 21026

Micro-hydrogel molding-assisted fabrication of a PDMS-based microfluidic concentration-gradient generator for dynamic anticancer drug testing†

Dhruba Dhar, Jyotirmoy Chatterjee and Soumen Das *

Traditional drug testing *via* polystyrene or glass-based cell culture platforms exposes cells to static drug doses and mechanically rigid environments [stiffness in gigapascals (GPa)], which do not accurately replicate physiological conditions. To address these limitations, we developed a polydimethylsiloxane (PDMS)-based microfluidic concentration gradient generator (μCGG) with six integrated cell culture chambers, using a cost-effective and frugal micro-hydrogel molding-assisted technique that eliminates the need for cleanroom infrastructure, specialized equipment, or advanced expertise. This platform facilitates dynamic drug exposure to cells cultured in chambers with flexible PDMS bases [stiffness in kilopascal (kPa) range], providing a scalable and accessible approach for drug dose–response analysis under physiologically relevant conditions, thereby improving accuracy. μCGG utilized a pressure-driven flow design that repeatedly split, mixed, and recombined fluid streams owing to the presence of the mesh-like geometry of the microchannels. This generated a stable and predictable drug concentration gradient across six outlet chambers, as validated through COMSOL simulations, fluorescence microscopy, and UV-Vis spectroscopy using 5-fluorouracil (5-Fu) as a model drug. MDA-MB-231 breast cancer cells were then cultured in the outlet chambers and exposed to six distinct dynamically generated concentrations of 5-Fu. Cellular viability assessed *via* live/dead assays yielded an IC_{50} value of 41 ± 4 μM, closely matching the results from conventional multiwell plates using manually pipetted gradients under static conditions (IC_{50}: 36 ± 3 μM). Additional validation was carried out using immunocytochemistry and flow cytometry to assess apoptotic markers and treatment responses. Overall, our study presents a simple, frugal, and scalable microfluidic platform that addresses the major limitations of traditional drug testing platforms by incorporating dynamic chemical gradients, physiologically relevant mechanical environments, and low-barrier fabrication methods, paving its way for broader adoption in preclinical drug evaluation and dose–response assays.

Received 29th March 2025
Accepted 6th June 2025

DOI: 10.1039/d5ra02192h

rsc.li/rsc-advances

Introduction

Cells typically reside in microenvironments characterized by varying concentration gradients of biomolecules. These gradients play critical roles in regulating biological processes, such as development, embryonic growth, immune response, cancer metastasis, and wound healing.[1] Understanding the interplay between biochemical gradients and cellular signaling pathways is the key to unraveling the mechanisms underlying the human body functions. Over the years, various *in vitro* systems, such as culture flasks, Boyden chambers, Dunn slide chambers, multiwell plates, Zigmond chambers, and Petri dishes, have been widely used to mimic the *in vivo* concentration gradients of biomolecules. These systems have been instrumental in examining the impact of such gradients on processes such as cell migration, cell differentiation, and drug resistance. Additionally, they have been exploited for drug dose–response analysis, *in vitro* expression of proteins, toxicity assessments of heavy metals, and detection of enzymatic kinetics. However, they have several limitations that hinder their ability to accurately replicate physiological conditions. One major drawback is that they expose cultured cells to static drug concentrations, failing to recreate the dynamic and transient gradients experienced in real biological environments, leading to less predictive outcomes. Additionally, polystyrene, the most commonly used material for traditional cell culture platforms, has an elastic modulus of approximately 3 GPa, making it significantly stiffer than most biological tissues, thereby failing to provide physiologically relevant mechanical conditions for cells.[2] Another limitation is their larger operational scale (ranging from millimeters to centimeters) compared with the relevant length scales of the cytokine/chemokine gradients produced in living cells (approximately 250 μm).[1,3] These challenges highlight the need

School of Medical Sciences and Technology, Indian Institute of Technology Kharagpur, Kharagpur, India. E-mail: sou@smst.iitkgp.ac.in

† Electronic supplementary information (ESI) available. See DOI: https://doi.org/10.1039/d5ra02192h

for advanced *in vitro* platforms that can better mimic biochemical gradients, tissue mechanics, and microenvironmental factors, offering more realistic and predictive models for biomedical research and drug development. In this direction, microfluidic concentration gradient generators (μCGG) have emerged as a viable alternative to conventional drug testing platforms, facilitating the creation of dynamic concentration gradients with higher resolution. In addition, these platforms provide several benefits, such as precise control over hydrodynamic and mass transport conditions, ease of customization, low reagent consumption, portability, efficient sample utilization, high surface-to-volume ratio, and automation.

μCGGs represent a diverse category of devices capable of generating biochemical concentration gradients using two approaches: mono-phase methods (such as tree-shape, altered tree-shape, membrane-based, Y-shaped, and pressure balance-based methods) and droplet-based methods (including droplet generation, droplet coalescence, and droplet mixing).[4] Recently, these platforms have been extensively studied and applied in diverse experiments, facilitating the investigation of numerous biological phenomena, such as cancer invasion,[5] angiogenesis,[6,7] drug resistance,[8] hypoxia/oxygen gradients,[9,10] and shear stress.[11] Additionally, these platforms have been explored for conducting drug dose–response analysis, offering critical insights into their anti-cancer efficacy.[12,13] The precise analysis of therapeutic dosages of novel or repurposed drugs using μCGG offers a promising alternative to the sluggish, laborious, and error-prone multiwell-based drug testing process, which primarily relies on manual pipetting for customized gradient generation. Although photolithography has traditionally been the primary fabrication method for existing state-of-the-art μCGGs,[14] its dependence on cleanroom environments and labor-intensive manual procedures has led to a growing interest in stereolithography (SLA) 3D printing as an alternative.[15,16] However, most 3D-printed μCGGs use photopolymer resins, which often fail to accurately replicate the biological properties of tissues owing to their lack of flexibility, porosity, and mechanical characteristics that are essential for mimicking tumor behavior *in vivo*.[17] Furthermore, many SLA resins are not fully biocompatible, impacting cell viability, adhesion, differentiation, and long-term cell culture within the printed constructs. Additionally, their restricted optical transparency further complicates sample visualization, limiting their effectiveness in biological studies.[18] This has led researchers to often use 3D-printed resin molds to fabricate polydimethylsiloxane (PDMS)-based microfluidic devices;[19] however, this multi-step process adds complexity, faces scalability limitations, incurs high costs, and necessitates extensive post-processing requirements, which further hinder accessibility, reproducibility, and commercial viability, making high-throughput drug dose–response analysis challenging. Consequently, the focus has shifted toward fabrication techniques that are simple and inexpensive and do not require high-end instrumentation.[7]

To address these limitations, herein, we design and fabricate a PDMS-based μCGG using a frugal lithography-free and cleanroom-free micro-hydrogel molding-assisted technique.[20,21] The on-chip device featured a two-inlet-sixteen outlet configuration with a grid of microchannels intersecting each other, forming a mesh-like pattern. Six cylindrical hollow chambers, strategically positioned at six selected outlets, were designed to facilitate cell culture under dynamic conditions. To better mimic physiological stiffness, the base of these chambers was fabricated using 20 : 1 (prepolymer-to-crosslinker ratio) PDMS instead of conventional polystyrene or glass, providing mechanical stiffness values in the kPa range similar to those found in native tissues. μCGG, designed based on pressure-driven flow systems, repeatedly splits, mixes, and recombines fluid streams owing to the presence of the mesh-like arrangement of the microchannels, generating a stable dynamic concentration gradient of 5-fluorouracil (5-Fu, used as a model drug). This phenomenon was validated both theoretically using COMSOL simulations and experimentally *via* fluorescence microscopy and UV-Vis spectroscopy studies. Subsequently, the efficacy of the *in vitro* drug testing device was assessed on MDA-MB-231 cells using live/dead assays, yielding IC_{50} values (41 ± 4 μM) similar to those obtained through conventional multiwell plates (IC_{50}: 36 ± 3 μM). Further, validation was carried out using immunocytochemistry and flow cytometry to assess proliferation/apoptotic markers and treatment response. Overall, this platform facilitates dynamic drug exposure to cells cultured on PDMS substrates with mechanical characteristics in the kPa range, offering a scalable and accessible approach for *in vitro* drug testing under physiologically relevant conditions, thereby enhancing the accuracy of drug efficacy assessments.

Methodology

Theoretical exploration and optimisation of device design parameters

Prior to device fabrication, we conducted *in silico* simulations using COMSOL Multiphysics software (v5.3) to strategically reduce iterative trial-and-error during prototyping. These simulations were instrumental in assessing the performance of the proposed μCGG design and optimizing key parameters, such as microchannel geometry, node spacing, and overall layout, to ensure the efficient generation of chemical gradients. Detailed descriptions of the simulation methodology are provided in the ESI† under the section: optimisation of design parameters and drug concentration gradient generation in μCGG platform using COMSOL simulations.

Design principle. The on-chip platform design proposed in this study is based on pressure-driven systems, similar to the tree-shaped network architecture.[22] The fundamental concept behind creating a concentration gradient using this design entails designing an intricate mesh-like arrangement of intersecting microchannels that allows for the repeated splitting and recombination of flowing streams within them. During each stage, streams are divided and directed into adjacent branch channels of the next stage with predetermined ratios at the point of bifurcation. After thorough mixing, neighboring branch streams combine to form new concentrations, while the concentrations of the two outermost branch streams remain constant in the final stage. The growing number of branches

results in a wider array of concentrations by repeatedly splitting, combining, and mixing at each step.

Lithography-free and clean-room-free fabrication of μCGG

To fabricate the finalized μCGG design, a frugal lithography-free and clean-room-free micro-hydrogel molding-assisted fabrication technique was employed,[20,21] wherein the design consisted of two parts: a grid of microchannels for media flow and concentration gradient generation and adjacent cylindrical hollow chambers for cell culture. The technique for fabricating the microchannels and adjacent cylindrical hollow chambers closely follows the approach previously published by our group.[20,21] The fabrication procedure is briefly outlined as follows.

Substrate preparation. First, PDMS was prepared by mixing the base elastomer and curing agent (Sylgard 184, Dow Corning Chemicals, Kevin Electrochem, India) at a 20 : 1 ratio (to replicate the physiological stiffness; kPa),[20] followed by degassing (until bubbles disappeared) the mixture using a vacuum pump. The replication of physiologically relevant stiffness using this 20 : 1 polymer-to-crosslinker ratio was further validated through atomic force microscopy (AFM) analysis. Detailed results of this mechanical characterization are provided in the ESI† under the section: mechanical characterization of PDMS using AFM.

The prepared PDMS mixture was then spin-coated on a clean 60 mm polystyrene Petri dish at 600 rpm for 20 seconds using a spin coater [Fig. 1a(i)]. Further, the coated Petri dishes were cured at 60 °C for 6 h in an oven. The as-prepared PDMS-coated Petri dishes were used as the base substrate/mold for device fabrication.

Preparation of agarose solution, gel wires, and gel chips. To prepare the hydrogel molds, a solution of 16% v/v glycerol and 1 mg mL^{-1} food color dye (red) dissolved in Milli-Q deionized (DI) water was first prepared. 2.5% w/v of agarose powder was poured into this solution, and the final volume was adjusted to 20 mL. The prepared colored hydrogel mixture was poured into a conical flask and heated in a microwave oven for 30–45 seconds until the contents were completely dissolved. A part of the hydrogel mixture was then filled in the Tygon tubing with an inner diameter of 500 μm using a syringe to prepare the hydrogel wires, and from the remaining mixture, 0.47 mL solution was poured into a 35 mm × 15 mm Petri dish to prepare flat gel chips of ~500 μm thickness. The Petri dish and the tubing were then kept at 4 °C for 10 minutes for gelation.

Patterning. A precise design layout with accurate dimensions was first printed on paper to serve as a stencil or reference and was placed beneath the Petri dish to guide the placement process. Subsequently, one end of the hydrogel-filled tubing was connected to a syringe and pneumatically pushed to eject the hydrogel wires onto the PDMS-coated Petri dishes fabricated earlier. The ejected hydrogel wires were then manually arranged into the desired pattern by tracing the printed layout to ensure the accuracy and reproducibility of the design parameters. After this, the PDMS-coated Petri dish with the patterned hydrogel wires was placed on a hotplate at 80 °C for 30 seconds for the hydrogel wires (which are arranged

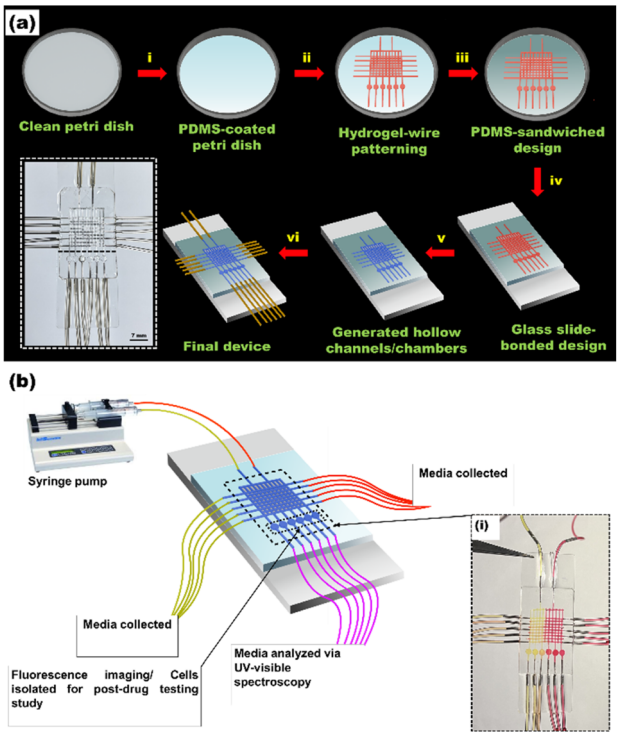

Fig. 1 (a) Schematic of the fabrication process of the microfluidic gradient generator: (i) spin coating of PDMS pre-polymer [at 20 : 1 (polymer : crosslinker)] on the Petri dish at 600 rpm for 20 seconds, (ii) patterning of the hydrogel wires/chips (composed of 2.5% w/v agarose, 16% v/v glycerol and 1 mg mL^{-1} red food color) by tracing the printed design (solidified wires/chips denoted in red color in the image for ease of visualization purpose), (iii) second layer of PDMS prepolymer (20 : 1) poured to sandwich the wires/chips inside the PDMS, (iv) cured PDMS block with the embedded design cut and bonded to a glass slide, (v) removal of hydrogel wires/chips by gently flushing hot water, leading to the generation of hollow microchannels and chambers (blue colored wires/chips signifies their hollow nature), and (vi) inlets and outlets connected to the channels (denoted by the yellow colored wires) [inset: snapshot of the final prepared device]. (b) Schematic of the experimental setup: (i) snapshot of the actual device in dynamic conditions, where red and yellow dye color solutions (both at 1 mg mL^{-1}) signify media with two different drug concentrations.

perpendicular to one another) initially present on top of one another on different planes to merge and form a single unit in a single plane. This was followed by cutting the gel chips using a 2.5 mm diameter biopsy puncture and arranging them on the glass slides to obtain the final design [Fig. 1a(ii)]. Subsequently, the entire design was covered with additional PDMS prepolymer (1.5 g) and kept undisturbed on a flat surface for 5 minutes for the uniform spreading of the added PDMS layer [Fig. 1a(iii)]. This was followed by curing the Petri dishes at 45 °C on a hot plate for 12 hours.

Device preparation. Once the second PDMS layer was fully cured, the PDMS block containing the embedded design was meticulously cut and separated from the mold. In the next step, the PDMS block was permanently bonded to a glass slide [Fig. 1a(iv)]. Before bonding, the glass slide's top surface and the PDMS block's bottom surface were treated with oxygen plasma at 40 W RF power (FEMTO version, Diener Electronics,

Germany) for 30 seconds. The additional step of transferring the microfluidic device from the Petri dish to a glass slide was performed to facilitate a convenient connection of the inlets and outlets to the microfluidic channels, enabling easier fluid handling and interfacing. Additionally, the transparent glass slide provided an optimal substrate for capturing high-quality microscopy images of the microfluidic device and the experiments being conducted within it. This was followed by the removal of the hydrogel wires and chips sandwiched within the PDMS layers by gently flushing hot water, leading to the generation of hollow microchannels and adjacent hollow PDMS chambers [Fig. 1a(v)]. Subsequently, in-house developed inlets and outlets were inserted into the device, and connections were sealed with PDMS prepolymer [Fig. 1a(vi)].

Characterization of the fabricated on-chip platform

Micro-CT analysis. To characterize the depth and 3D structure of the device, micro-computed tomography (micro-CT, GE Phoenix v|tome|x, Germany) was performed to obtain a 3D scan (at 1000 scan slices) of the device without the attached inlets and outlets. The instrument was operated at 90 kV, current: 40 mA, and 3.8 μm of voxel size (resolution).

AFM analysis. The surface roughness of the individual microchannels, nodes (microchannel intersections), and cell culture chambers was investigated using AFM [Oxford Asylum MFP 3D]. For this, the on-chip platform was fabricated directly on a clean Petri dish [skipping the PDMS spin-coating of the Petri dish step shown in Fig. 1a(i) to avoid embedding of the hydrogel wires/chips within PDMS], followed by peeling off the cured PDMS layer, exposing the inner surface of the microchannels/nodes/cell culture chambers, thus guaranteeing the accessibility of these surfaces for analysis. The topography of the different regions of the fabricated platform was imaged in contact mode using a silicon nitride cantilever tip.

Experimental validation of drug concentration gradient generation

Evaluation of gradient generation using fluorescence microscopy. The gradient generation phenomenon was experimentally validated using fluorescence microscopy. This was done by perfusing (at flow rate: $I_1 = I_2 = 10\ \mu L\ min^{-1}$) a fluorescent dye CellTracker™ Blue CMAC (Catalogue number: C2110, Invitrogen) at 100 μM concentration from I_1 and 0 μM from I_2 for 48 hours and subsequently measuring the fluorescence intensities generated at the different cell culture chambers using a Nikon Eclipse TS2R epifluorescence microscope. This dye was chosen because of its similarity in molecular weight to 5-Fu (5-Fu M_w: 130.078 g mol^{-1}, CMAC M_w: 209.6 g mol^{-1}). The experimental flow setup is depicted in Fig. 1b, where the two different color solutions [red and yellow, Fig. 1b(i)] denote the different drug concentrations of the perfused media.

Evaluation of 5-Fu concentration gradient generation using UV-vis spectroscopy

Initially, a 500 μM stock solution of 5-Fu was prepared by dissolving it in cell culture media. This stock solution was subsequently diluted to generate various concentrations (0–120 μM) of 5-Fu, followed by calculating the absorbance values for each of the prepared 5-Fu concentrations using a UV-vis spectrophotometer (UV-1800, Make: Shimadzu) at 266 nm. Subsequently, a standard curve was prepared, with the concentration of 5-Fu plotted on the *x*-axis and the absorbance values on the *y*-axis. The unknown concentrations of 5-Fu were determined from the samples collected from the different outlets (under the conditions: $I_1 = I_2 = 10\ \mu L\ min^{-1}$; 5-Fu concentration at I_1: 100 μM and I_2: 0 μM) by measuring the UV absorbance values at 266 nm and using the standard curve.

Cell culture and on-chip assessment of dynamic drug gradients for drug dose–response analysis

Cell culture. MDA-MB-231 cells purchased from the National Centre for Cell Science (NCCS), Pune were cultured inside hollow PDMS chambers of mechanical stiffness in the kPa range to assess the device's capacity to expose the cells to a drug gradient for precise drug dose–response analysis under dynamic conditions. The first step involved priming the PDMS surface within the hollow chambers for cell attachment. This was done by treating the fabricated device with O_2 plasma for 3 minutes at 70 W RF power using a plasma cleaner (FEMTO version, Diener Electronics, Germany) to convert the hydrophobic PDMS surface to hydrophilic.[20] Subsequently, a mixture of rat tail collagen I (100 μg mL^{-1}; ThermoFisher Scientific) and fibronectin (30 μg mL^{-1}; ThermoFisher Scientific) was injected into the device, followed by incubation at 37 °C for 2 hours.[23] MDA-MB-231 cells in their logarithmic growth phase were then introduced into hollow chambers at 2000 cells per chamber. The cell-seeded device was then incubated at 37 °C under a humidified (5% CO_2) atmosphere for 1 hour to facilitate cell attachment. Following this, the cells were grown in DMEM medium, added with 10% FBS and 1% penicillin–streptomycin antibiotic, and perfused at a 10 μL per minute flow rate using a syringe pump (Cole-Parmer, India) for 24 hours at 37 °C under a humidified atmosphere. For the cell culture studies under flow conditions, we restricted the flow rate to 10 μL per minute to protect the cells from hydrodynamic shear.[24]

Cell viability analysis. Briefly, MDA-MB-231 cells initially cultured for 24 hours under flow conditions (10 μL per minute) were exposed to a 5-Fu gradient by perfusing media containing 100 μM of 5-Fu through one inlet, while media without any drug was perfused through another inlet for 48 hours. The impact of the drug gradient on cell viability was assessed using a differential nuclear staining (DNS) assay.[25] This involved incubating the cells (under static conditions) for 30 minutes with 1 μg mL^{-1} Hoechst-33342 stain and 2 μg mL^{-1} propidium iodide (PI) by gently perfusing the dye-containing medium inside the device. This was followed by capturing the fluorescence images using a Nikon Eclipse TS2R microscope.

Further, the total number of live cells (N_{Live}) was determined by subtracting the number of nuclei stained with Hoechst-33342 and the number of PI-stained dead nuclei. The measurements were performed using ImageJ software.

$$\text{Cell viability (\%)} = \frac{N_{\text{live}} \text{ in the drug-treated samples}}{\text{number of cells in control}} \times 100 \quad (1)$$

Immunocytochemistry analysis of drug effect. To demonstrate a post-drug exposure immunocytochemistry study in the device, we examined the impact of the drug gradient on the proliferation potential of MDA-MB-231 cells by evaluating the expression profile of Ki-67, a well-known nuclear protein present in proliferating cancer cells.[26] This was accomplished by fixing the MDA-MB-231 cells using a 3.5% paraformaldehyde solution for 15 minutes at room temperature after they had been exposed to a 5-Fu gradient for 48 hours under flow conditions (10 μL per minute). Following fixation, the cells were washed three times with 0.1 M glycine/1× phosphate-buffered saline (PBS). The samples were then permeabilized with 0.2% Triton X-100 prepared in 1× PBS for 20 minutes. Subsequently, blocking was performed to inhibit non-specific binding using 2% bovine serum albumin/0.2% Triton X-100 for 30 minutes, followed by treating the cells overnight at 4 °C with a primary antibody against Ki-67 (Catalogue no.-A11390, Abclonal) at a 1 : 200 dilution. The cells were then incubated with goat anti-rabbit Alexa Fluor 488 (Invitrogen, A27034) secondary antibody at a 1 : 1000 dilution for 1 hour at room temperature. Following this, the cells were washed with 1× PBS and then subjected to nuclei staining using 4′,6-diamidino-2-phenylindole (DAPI) for 10 minutes, followed by again washing them with 1× PBS. The steps performed, from fixing to staining, were performed in the absence of any flow. Subsequently, fluorescence images were taken using an Olympus FV3000 confocal microscope.

Analysis of apoptosis *via* flow cytometry. As per the available literature, only a limited number of on-chip models currently exist that enable the study of cells isolated from the device after drug gradients have been applied. Consequently, we performed flow cytometry studies to showcase the platform's potential for analyzing the device-isolated cells in response to drug exposure. In a subset of corresponding experiments, we tested the extent of apoptosis induction in the cell post-exposure to 5-Fu at a concentration lower than the IC_{50} value. The study was performed at a single concentration exposure per device by perfusing 5-Fu at a 35 μm concentration through both inlets rather than as a gradient. This allowed for the pooling of cells from all six chambers to obtain a suitable cell concentration for flow cytometry analysis. Briefly, MDA-MB-231 cells cultured inside hollow chambers were treated with 5-Fu (at 35 μm) for 48 hours under flow conditions. Our control group involved culturing the cells for 48 hours after perfusing the media without any drug from both inlets. This was followed by cutting the device along the dark blue dashed line marked in Fig. 1b (inset). The cells were then trypsinized and isolated from the individual hollow chambers by gently perfusing 0.25% trypsin–EDTA solution and incubating for 3 minutes. Subsequently, the cells isolated from the chambers/outlets were transferred to a 1.5 mL Eppendorf tube and centrifuged at 2000 rpm for 3 minutes to pellet down the cells. The pelleted cells were then stained with Annexin V-FITC and PI by following the manufacturer's protocol [Annexin V-FITC/PI apoptosis kit (Catalogue no.: BMS500FI-100), Invitrogen] and kept on ice in the darkness until flow cytometry analysis.

Scalability of the device

The frugal micro-hydrogel assembling-assisted fabrication technique employed for generating the mesh pattern is both spontaneous and scalable. Tygon tubings of different diameters can be used to generate hydrogel wires, which in turn can be used to fabricate microchannels of different cross-sectional diameters and nodes of various sizes. To illustrate the potential of the fabrication technique in upscaling or downscaling channel layouts, we fabricated devices of varying sizes and designs or inlet/outlet configurations using Tygon tubings of 800 μm and 250 μm inner diameters.

Statistical analysis

All statistical analyses were performed using GraphPad Prism version 8.0.2. For comparisons involving single variables across multiple groups, a two-way analysis of variance (ANOVA) was employed, followed by Tukey's post hoc test for multiple comparisons with a 95% confidence interval. The results are expressed as the mean ± standard error of the mean (SEM), with significance thresholds set as follows: $***P \leq 0.001$, $**P < 0.05$, and $*P < 0.02$. A P value > 0.05 was considered statistically non-significant (ns).

Results

Theoretical validation of design parameters and drug concentration gradient generation

Initially, we focused on optimizing the μCGG device geometry using *in silico* studies to ensure effective drug gradient generation, using 5-Fu as a model drug, while ensuring the design remained feasible for fabrication using the frugal micro-hydrogel molding-assisted technique. This theoretical exploration enabled us to finalize a robust design prior to fabrication, thereby conserving time, resources, and effort during subsequent experimental validation.

To achieve this, we conducted a series of simulations using "laminar flow" and "transport of diluted species" physics domains, focusing on adjusting the spacing between the horizontally and vertically arranged microchannels within the grid. A minimum separation distance of 1000 μm was maintained between these channels to allow sufficient spacing for proper placement during fabrication. Based on these simulations, we finalized the design parameters [Fig. S1†], which provided a well-defined concentration gradient and ensured sufficient room for the precise manual placement of individual hydrogel wires during fabrication. Using these optimized parameters, we numerically simulated the 5-Fu concentration profile at a flow rate of $I_1 = I_2 = 10\ \mu L\ min^{-1}$, with 5-Fu concentrations fixed at $I_1 = 100\ \mu M$ and $I_2 = 0\ \mu M$ for all cases. Analysis of the concentrations at different outlets revealed a uniformly declining concentration gradient pattern at outlet 1–6 (Fig. 2a), with four distinct intermediate concentrations between the highest and

lowest drug levels. In contrast, the concentration profiles at outlet a–e and f–j displayed gradients of 96.9–100 μM and 0–4.8 μM, respectively, closely matching the media perfused through I_1 and I_2 (Fig. 2b). Consequently, outlet 1–6 were selected to integrate the cell culture chambers for further *in vitro* drug dose–response studies, while outlet a–j were deemed unsuitable for this purpose. Additionally, we examined the impact of varying flow rates ($I_1 = I_2 = 10$ μL min^{-1}; $I_1 = 20$ μL min^{-1}, $I_2 = 10$ μL min^{-1}; $I_1 = 10$ μL min^{-1}, $I_2 = 20$ μL min^{-1}; $I_1 = I_2 = 50$ μL min^{-1}; $I_1 = I_2 = 100$ μL min^{-1}) on gradient formation (Fig. 2c). The results confirmed that equal flow rates at both inlets were essential for generating a stable and well-defined concentration gradient. Finally, we conducted simulations using the finalized design with incorporated cell culture chambers at $I_1 = I_2 = 10$ μL min^{-1} for up to 48 hours (Fig. 2d) and measured the simulated concentration profiles along a central line spanning through the cell culture chambers, as depicted in Fig. 2e.

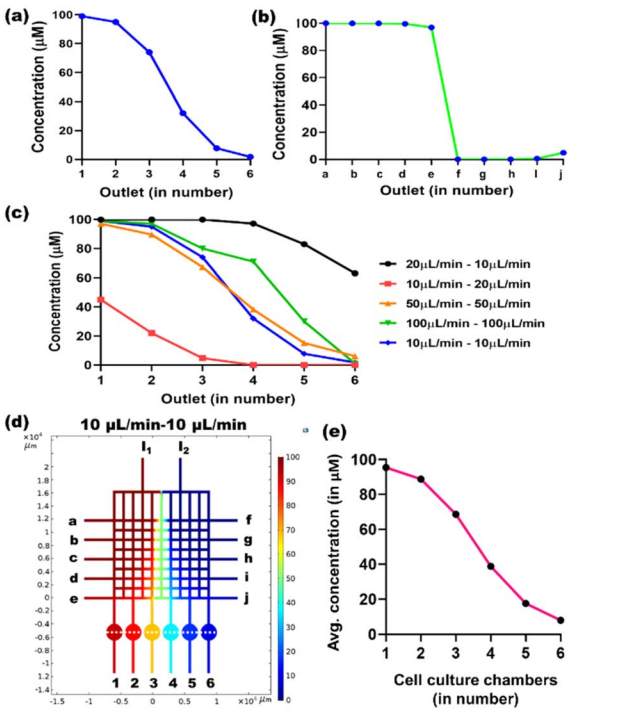

Fig. 2 Theoretical validation of 5-Fu gradient generation using COMSOL multiphysics software. (a) Simulated 5-Fu concentrations at outlets 1–6 within the optimized 2D geometry at a flow rate of $I_1 = I_2 = 10$ μL min^{-1}. (b) Simulated 5-Fu concentrations at outlets a–j at a flow rate of $I_1 = I_2 = 10$ μL min^{-1}. (c) Comparison of 5-Fu concentrations at outlets 1–6 under different flow conditions: $I_1 = 10$ μL min^{-1}, $I_2 = 20$ μL min^{-1}; $I_1 = 20$ μL min^{-1}, $I_2 = 10$ μL min^{-1}; $I_1 = I_2 = 10$ μL min^{-1}; $I_1 = I_2 = 50$ μL min^{-1}; and $I_1 = I_2 = 100$ μL min^{-1}. (d) Snapshot of the simulated 5-Fu concentration profile generated within the cell culture chamber-integrated design at $I_1 = I_2 = 10$ μL min^{-1} [red and blue colors indicate 5-Fu concentrations of 100 μM and 0 μM, respectively]. (e) Theoretical 5-Fu concentration distribution along a central line spanning the cell culture chambers, as indicated by white dashed lines in Fig. 2d: the concentrations are presented as the average values obtained along the central line of individual chambers (1–6).

Fabrication and characterization of the gradient-on-chip platform

Based on the optimized design parameters, μCGG was then fabricated using a lithography-free and cleanroom-free process, enabling the precise and cost-effective prototyping of the device (Fig. 1b). The fabrication process involved arranging hydrogel wires and chips according to the desired design by carefully tracing a printed layout to ensure precise placement. This led to the formation of a grid of microchannels for media flow/concentration gradient generation and adjacent cylindrical hollow chambers (six in number) possessing flexible PDMS bases of 9 ± 0.5 kPa (Fig. S2, ESI†) mechanical stiffness for test cell culture experiments. The fabricated platform with two inlets and sixteen connected outlets is depicted in Fig. 3a.

The developed μCGG was further characterized using AFM and micro-CT. AFM was used to measure local surface roughness across different regions of the platform over a 10 μm × 10 μm area, yielding an average roughness value of 2 ± 0.11 nm for the connecting microchannels [Fig. 3a(i)], 3 ± 0.14 nm for the channel intersections/nodes [Fig. 3a(ii)], and 2 ± 0.28 nm [Fig. 3a(iii)] for the cell culture chambers. Further, micro-CT analysis was performed, and the generated 3D images were analyzed using VGStudio MAX (Volume Graphics, Germany) software. The 3D reconstruction, along with cross-sectional views of the highlighted segments, is depicted in Fig. 3b. Analysis of the obtained images revealed that the fabricated

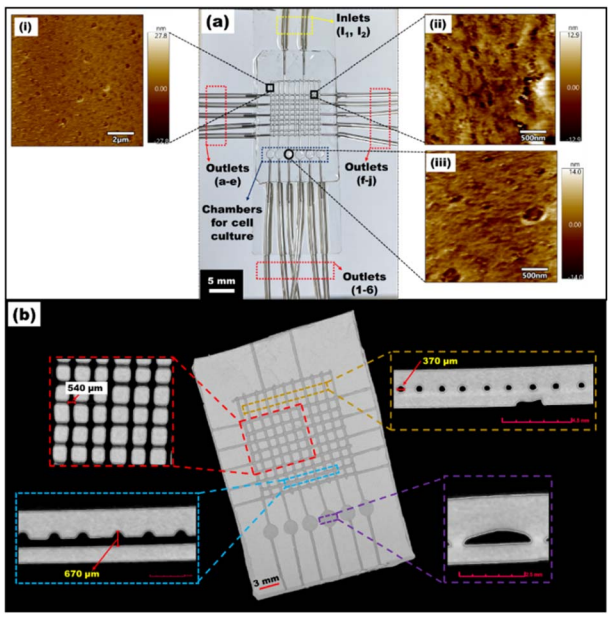

Fig. 3 Characterization of the fabricated μCGG platform. (a) Final gradient-on-chip platform with the inlets and outlets, (i–iii) analysis of surface roughness using AFM across various segments of the gradient-on-chip platform: measurement of local surface roughness was performed over a 10 μm × 10 μm area, yielding an average roughness value of (i) 2 ± 0.11 nm at the connecting microchannels, (ii) 3 ± 0.14 nm at channel intersections/nodes, and (iii) 2 ± 0.28 nm at the cell culture chambers. (b) Micro-CT generated 3D scan of the fabricated gradient-on-chip platform; inset: cross-sectional view of the highlighted segments.

microchannels had a diameter of approximately 370 μm, while the nodes formed at the channel intersections had a height of ~670 μm. Additionally, the adjacent hollow chambers measured 2.5 mm in diameter and ~480 μm in height.

Experimental validation of drug concentration gradient generation and comparison with *in silico* results

After fabricating μCGG, we validated the gradient generation capability of the platform by performing fluorescence microscopy of the cylindrical chambers connected at outlet 1–6. This involved perfusing 100 μM of CellTracker™ Blue CMAC dye (chosen because of its molecular weight's similarity with 5-Fu) through I_1 and 0 μM through I_2 (Fig. 4a). The obtained fluorescence images were analyzed using ImageJ software to extract the corresponding concentration profiles. This was done by converting the fluorescence images into 8-bit images and measuring the mean gray values using the command prompt Analyse >> Measure, followed by converting the mean gray values into concentrations (μM). The experimentally determined concentration profiles were then compared to those obtained through simulations, as presented in Fig. 4b. From the plots, it was observed that the experimentally determined gradients showed a similar trend to that observed using simulations.

Subsequently, the generation of a stable 5-Fu concentration gradient at outlet 1–6 was further validated using UV-visible spectroscopy (under the following conditions: $I_1 = I_2 = 10$ μL min^{-1}; 5-Fu concentration at I_1: 100 μM and I_2: 0 μM) by collecting (from the outlet 1–6) and measuring the absorbance values of the different samples at 266 nm. The concentrations of 5-Fu generated at the different outlets were then calculated from the linear regression equation of 5-Fu: $y = 0.006740x + 0.008272$ ($R^2 = 0.9994$; x = concentration of 5-Fu in μM, y = absorbance of 5-Fu at 266 nm) obtained from the 5-Fu standard curve (Fig. 4c). A comparison between the 5-Fu concentrations generated at the outlets (1–6), calculated experimentally using UV-visible spectroscopy and *via* simulations, is illustrated in Fig. 4d. The close proximity between the concentration values calculated experimentally and *via* simulation indicates the capability of our COMSOL model to predict the concentrations at the different outlets if the diffusion coefficients of the diffusing molecules are known.

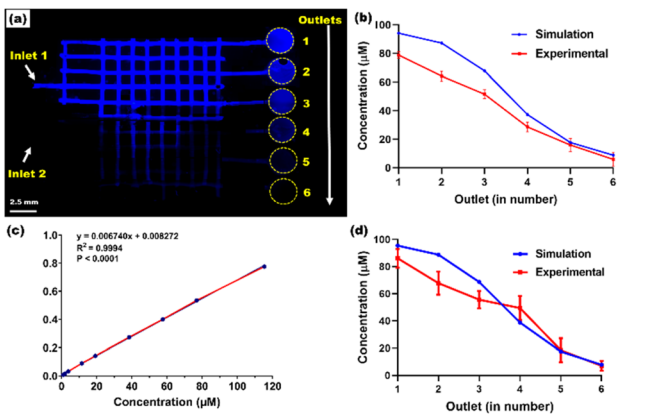

Fig. 4 Experimental validation of gradient generation using fluorescence microscopy and UV-visible spectroscopy. (a) Fluorescence image showing gradient formation at the cylindrical chambers along outlets 1–6 (highlighted with yellow dashed circles), generated by perfusing CellTracker™ Blue CMAC dye through inlet 1 and dye-free media through inlet 2 (not visible owing to the absence of fluorescence). (b) Comparison between the concentration profiles of the fluorescent dye obtained experimentally and those estimated theoretically across various chambers located along the outlets 1–6. (c) Linear standard curve of 5-fluorouracil, determined using UV-visible spectroscopy at a wavelength of 266 nm. (d) Comparison between the 5-Fu concentrations estimated from the 5-Fu standard curve and *via* simulation ($n = 3$).

Evaluation of the drug testing efficiency of the on-chip platform

To evaluate the functional performance of the device, we assessed its drug testing efficiency using the DNS assay, which involved staining cells with Hoechst-33342 and PI. Hoechst-33342 selectively stained the nuclei of live cells, producing blue fluorescence, while PI marked the nuclei of dead cells, resulting in red fluorescence. As the concentration of 5-Fu increased across the six cell culture chambers, with outlet 6 receiving the lowest 5-Fu concentration and outlet 1 the highest, we observed a progressive decrease in the number of Hoechst-stained (blue) nuclei and a corresponding increase in PI-stained (red) nuclei (from outlet 6 to outlet 1), confirming a dose-dependent cytotoxic effect (Fig. 5a). In the composite panel, the merged images of Hoechst-33342 and PI exhibit magenta-colored nuclei, indicating the co-localization of both fluorescence signals in the dead cells. Additionally, the cell viability (%) (Fig. 5b) resulting from exposure to the generated 5-Fu concentration gradient (0–100 μM) at the different outlets was estimated using eqn (1). Subsequently, an IC_{50} value of 41 ± 4 μM was determined from the cell viability (%) plot (Fig. 5b) using the GraphPad Prism software. For comparison, IC_{50} values were also calculated using conventional multiwell plates with manually pipetted drug gradients under static conditions, yielding a value of 36 ± 3 μM. This close agreement between the values obtained from our microfluidic device and the traditional methods validates the accuracy of our platform. Moreover, these results are consistent with the IC_{50} trends reported in previous studies.[27]

The effect of the drug gradient on the proliferation potential of MDA-MB-231 cells was then assessed using confocal fluorescence microscopy (Fig. 5c). This was done by analyzing the obtained fluorescent images using ImageJ software (open-source) to perform a qualitative assessment of the changes in Ki-67 expression profiles in response to the drug gradient. The process involved splitting the confocal images into different channels using the "split-channel" command to isolate the green channel, which is specific to Ki-67. The mean gray values were then extracted from 20 individual cells using the following command prompt: "analyse > measure." These values were averaged and subtracted from the mean gray value of a blank sample for baseline correction. This process was repeated three times across all datasets (*i.e.*, control and outlet 1–6), providing

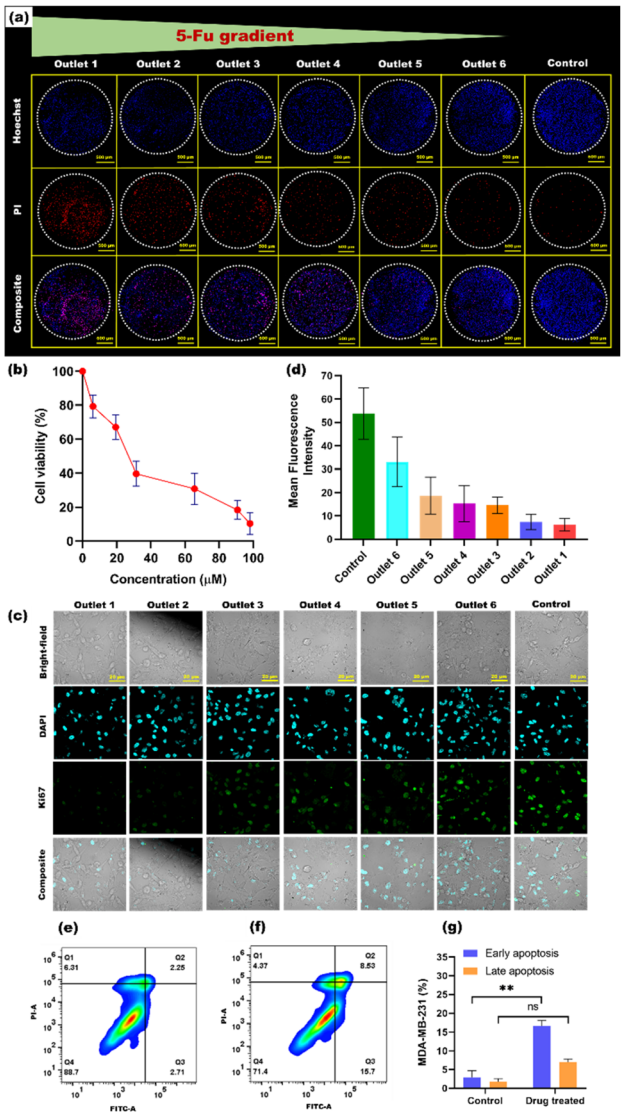

Fig. 5 (a) Evaluation of drug testing efficiency of the on-chip platform using live-dead assay, where the nuclei of the cells with intact plasma membranes were stained solely with Hoechst-33342 (blue color), while the nuclei of the cells with compromised cell membranes (magenta color) were stained with both Hoechst-33342 and propidium iodide stains. (b) Cell viability (%) of MDA-MB-231 cells at different 5-Fu concentrations generated in the cell culture chambers. (c) Immunocytochemistry analysis of Ki-67 expression in MDA-MB-231 cells exposed to a 5-Fu gradient for 48 hours: panels display DAPI-stained nuclei (blue), Ki-67 staining (green), and the composite merged image, highlighting cellular proliferation across different outlets (representative regions with comparable cell density were selected across all the outlets to enable consistent quantification of Ki-67 expression). (d) Analysis of Ki-67 fluorescence intensity profile in the MDA-MB-231 cells exposed to the 5-Fu gradient for 48 hours across different outlets. (e and f) Analysis of apoptosis induction using flow cytometry in MDA-MB-231 cells: (e) untreated control and (f) treated with 5-Fu drug (at 35 μm concentration) [Q1: necrotic cells, Q2: late apoptotic cells, Q3: early apoptotic cells, and Q4: viable cells]. (g) Quantitative comparison of early and late apoptotic cell populations between 5-Fu treated and untreated (control) MDA-MB-231 cells after 48 hours of exposure, as estimated using flow cytometry [data are presented as mean ± SEM; ***$P \leq 0.001$, **$P < 0.05$, *$P < 0.02$ A and ^{ns} P value > 0.05].

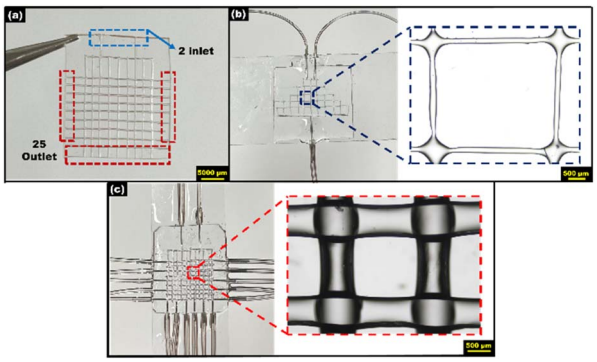

Fig. 6 (a) Fabricated 2-inlet–25-outlet mesh design (microchannel diameter: 370 μm). (b) Fabricated device featuring a tree-shaped design (microchannel diameter: ~180 μm). (c) Fabricated device with a microchannel diameter of ~700 μm.

the fluorescence intensity profile for Ki-67 expression. Consequently, as illustrated in Fig. 5d, the intensity of Ki-67 fluorescence decreased significantly across the various cell culture chambers compared to the control, demonstrating the detrimental effect of the drug gradient on the proliferation potential of cancer cells.

Further, the effects of the 5-Fu gradient on apoptosis induction within MDA-MB-231 cells were examined using flow cytometry by detecting Annexin V binding. The distribution (%) of the four cell populations, Q1: necrotic cells, Q2: late apoptotic cells, Q3: early apoptotic cells, and Q4: viable cells, is depicted in Fig. 4e and f. The findings revealed a notable presence of both early and late apoptotic cell populations (28.6%) following treatment (Fig. 4f) of the cells with 5-Fu (at a single concentration: 35 μm).

Scalability of μCGG

Finally, to demonstrate the high scalability and customization potential of the micro-hydrogel molding-based fabrication approach, enabling future adaptability in terms of the size and number of microchannels and nodes based on user requirements, we fabricated an on-chip mesh design featuring a 2-inlet, 25-outlet configuration (Fig. 6a) using Tygon tubing with an inner diameter of 400 μm. In addition to the mesh design, a tree-shaped design was also developed (Fig. 6b), incorporating microchannels with a diameter of ~180 μm, fabricated using Tygon tubing with an inner diameter of 250 μm. Furthermore, to highlight the versatility of this approach, larger microchannels (~700 μm in diameter) were fabricated using Tygon tubing with an inner diameter of 800 μm (Fig. 6c), underscoring the exceptional scalability of the fabrication process.

Conclusions and perspectives

In conclusion, we designed and developed a PDMS-based μCGG using an inexpensive and frugal lithography-free and clean room-free micro-hydrogel molding-assisted fabrication technique. This prototyping approach not only simplifies the fabrication of the μCGG device but also significantly reduces

reliance on expensive lithographic equipment and cleanroom facilities. Eliminating these technical and economic barriers enhances the accessibility and scalability of microfluidic device fabrication, particularly for laboratories with limited resources. Moreover, in contrast to other conventional approaches, such as using 3D printing,[19] which involves extensive and multi-step post-processing, along with high costs and scalability challenges, the hydrogel-based method presented herein offers a more straightforward and cost-effective alternative. This streamlined approach improves reproducibility and supports broader implementation, thereby ultimately advancing the goal of democratizing high-throughput drug dose response analysis and other advanced biomedical applications.

The fabricated device featured a two-inlet-sixteen outlet configuration and a grid of microchannels adjacent to cylindrical hollow chambers and employed a split/recombine strategy to generate the concentration gradients. The generation of a concentration (using 5-Fu as a model drug) gradient was theoretically validated using COMSOL simulation and experimentally *via* fluorescence microscopy and UV-Vis spectroscopy studies. Subsequently, the device was utilized to establish dynamic 5-Fu drug gradients, enabling dose–response studies on MDA-MB-231 cells cultured within cylindrical chambers made of PDMS substrates engineered to mimic physiological stiffness (9 ± 0.5 kPa). Subsequently, the cellular responses to the drug gradients were systematically analysed through live/dead staining, immunocytochemistry, and flow cytometry studies. The live/dead assays yielded an IC_{50} value of 41 ± 4 μM, which closely matched the IC_{50} value obtained from conventional multiwell plate-based static cultures (IC_{50}: 36 ± 3 μM). Unlike traditional static systems, μCGGs offer a more physiologically relevant microenvironment by mimicking the dynamic chemical concentration gradients present *in vivo*. Furthermore, the platform allows fine-tuning of gradient profiles to suit specific experimental needs by simply adjusting the flow rates and inlet concentrations.

Moreover, based on the outcomes achieved in this study, future investigations could explore the integration of cancer cells embedded in tissue-mimicking extracellular matrices or patient-derived organoids into cylindrical chambers. This would allow for the assessment of mono- or combinatorial-drug gradients in a more physiologically relevant context, enabling better recapitulation of drug delivery dynamics in deep tumor regions and more accurate evaluation of dose–response parameters.[28] Additionally, incorporating transepithelial electrical resistance (TEER) measurements could provide a quantitative metric of drug-induced toxicity under both mono- and co-culture-conditions or in patient-specific cultures, further enhancing the platform's potential for high-throughput drug screening applications.[29]

Furthermore, the simplicity and scalability of the fabrication procedure were evaluated, leading to the production of different designs, inlet–outlet configurations, and microchannels of different diameters and sizes. Thus, future investigations could explore expanding the design by incorporating additional horizontal and vertical microchannels, thereby enhancing the resolution of the concentration gradient. This modification would enable the generation of finer, more gradual concentration reductions, making the platform suitable for high-throughput and precise drug testing applications. Additionally, automating the arrangement of hydrogel wires, rather than relying on manual placement, could further improve the reproducibility and scalability of the fabrication process.

Data availability

All the data supporting the findings of this study are included in the main manuscript and the ESI.† No additional data are available beyond what is presented in this publication.

Author contributions

D. D.: conceptualization, methodology, investigation, data curation, formal analysis, writing – original draft; J. C.: resources, supervision; S. D.: resources, funding acquisition, supervision, writing – review & editing.

Conflicts of interest

There are no conflicts to declare.

Acknowledgements

The authors would like to thank CRF and the Department of Bioscience and Biotechnology, IIT Kharagpur, for the Micro-CT and Confocal microscopy facilities, respectively. The authors are also grateful to Dr Gayatri Mukherjee and Ms Debarati Biswas for helping with the flow cytometry studies. D. D. thanks Dr Jyotsana Priyadarshani, a postdoctoral researcher at KU Leuven, Belgium, for her guidance on the device's fabrication process. The authors would like to acknowledge Miss Akashlina Basu for her advice and help with the preparation of the illustrations. D. D. would like to thank the Ministry of Education (MoE) and IIT Kharagpur for providing the research fellowship.

References

1 A. G. G. Toh, Z. P. Wang, C. Yang and N.-T. Nguyen, *Micro and Nano*, 2014, **16**, 1–18.
2 N. Fekete, A. V. Béland, K. Campbell, S. L. Clark and C. A. Hoesli, *Transfusion*, 2018, **58**, 1800–1813.
3 S. Micheli, P. Mocellin, M. Sorgato, L. Bova and E. Cimetta, *Biochem. Eng. J.*, 2022, **181**, 108415.
4 X. Wang, Z. Liu and Y. Pang, *RSC Adv.*, 2017, **7**, 29966–29984.
5 M. Samandari, L. Rafiee, F. Alipanah, A. Sanati-Nezhad and S. H. Javanmard, *Sci. Rep.*, 2021, **11**(1), 1–11.
6 H. H. Hsu, P. L. Ko, C. C. Peng, Y. J. Cheng, H. M. Wu and Y. C. Tung, *Mater. Today Bio*, 2023, **21**, 100703.
7 S. Yadav, P. Tawade, K. Bachal, M. A. Rakshe, Y. Pundlik, P. S. Gandhi and A. Majumder, *Biomicrofluidics*, 2022, **16**, 064103.
8 A. Wu, K. Loutherback, G. Lambert, L. Estéèez-Salmerón, T. D. Tlsty, R. H. Austin and J. C. Sturm, *Proc. Natl. Acad. Sci. U. S. A.*, 2013, **110**, 16103–16108.

9 J. Grant, E. Lee, M. Almeida, S. Kim, N. LoGrande, G. Goyal, A. M. Sesay, D. T. Breault, R. Prantil-Baun and D. E. Ingber, *Lab Chip*, 2022, **22**, 1584.
10 S. F. Lam, V. S. Shirure, Y. E. Chu, A. G. Soetikno and S. C. George, *PLoS One*, 2018, **13**, e0209574.
11 A. Jaberi, A. Monemian Esfahani, F. Aghabaglou, J. S. Park, S. Ndao, A. Tamayol and R. Yang, *ACS Appl. Bio Mater.*, 2020, **3**, 6661–6671.
12 K. Bachal, S. Yadav, P. Gandhi and A. Majumder, *Lab Chip*, 2023, **23**, 261–271.
13 J. Kim, D. Taylor, N. Agrawal, H. Wang, H. Kim, A. Han, K. Rege and A. Jayaraman, *Lab Chip*, 2012, **12**, 1813–1822.
14 M. R. Carvalho, D. Barata, L. M. Teixeira, S. Giselbrecht, R. L. Reis, J. M. Oliveira, R. Truckenmüller and P. Habibovic, *Sci. Adv.*, 2019, **5**(5), eaaw1317.
15 E. Sweet, B. Yang, J. Chen, R. Vickerman, Y. Lin, A. Long, E. Jacobs, T. Wu, C. Mercier, R. Jew, Y. Attal, S. Liu, A. Chang and L. Lin, *Microsyst. Nanoeng.*, 2020, **6**(1), 1–14.
16 C. Heuer, J. A. Preuss, M. Buttkewitz, T. Scheper, E. Segal and J. Bahnemann, *Lab Chip*, 2022, **22**, 4950–4961.
17 S. Gallegos-Martínez, D. Choy-Buentello, K. A. Pérez-Álvarez, I. M. Lara-Mayorga, A. E. Aceves-Colin, Y. S. Zhang, G. Trujillo-De Santiago and M. M. Álvarez, *Biofabrication*, 2024, **16**, 045010.
18 E. Steinberg, R. Friedman, Y. Goldstein, N. Friedman, O. Beharier, J. A. Demma, G. Zamir, A. Hubert and O. Benny, *Commun. Biol.*, 2023, **6**(1), 1–14.
19 M. D. Poskus, T. Wang, Y. Deng, S. Borcherding, J. Atkinson and I. K. Zervantonakis, *Microsyst. Nanoeng.*, 2023, **9**(1), 1–15.
20 J. Priyadarshani, T. Roy, S. Das and S. Chakraborty, *ACS Biomater. Sci. Eng.*, 2021, **7**(3), 1263–1277.
21 D. Dhar, J. Chatterjee and S. Das, Indian Patent 202431091154, 2024.
22 M. D. Hossain Khan, S. A. Roberts, J. R. Cressman and N. Agrawal, *IEEE Healthcare Innovations and Point of Care Technologies*, HI-POCT, 2017, vol. 2017, pp. 60–63.
23 B. Saha, T. Mathur, J. J. Tronolone, M. Chokshi, G. K. Lokhande, A. Selahi, A. K. Gaharwar, V. Afshar-Kharghan, A. K. Sood, G. Bao and A. Jain, *Sci. Adv.*, 2021, **7**, 5283–5304.
24 L. Wang, W. Liu, Y. Wang, J. C. Wang, Q. Tu, R. Liu and J. Wang, *Lab Chip*, 2013, **13**, 695–705.
25 C. Lema, A. Varela-ramirez and R. J. Aguilera, *Curr Cell Biochem*, 2011, **1**, 1.
26 S. Uxa, P. Castillo-Binder, R. Kohler, K. Stangner, G. A. Müller and K. Engeland, *Cell Death Differ.*, 2021, **28**(12), 3357–3370.
27 A. Sagara, K. Igarashi, M. Otsuka, T. Karasawa, N. Gotoh, M. Narita, N. Kuzumaki, M. Narita and Y. Kato, *PLoS One*, 2016, **11**, e0164250.
28 X. He, Y. Jiang, L. Zhang, Y. Li, X. Hu, G. Hua, S. Cai, S. Mo and J. Peng, *Front Bioeng Biotechnol*, 2023, **11**, 1190637.
29 E. M. Shaughnessey, S. H. Kann, H. Azizgolshani, L. D. Black, J. L. Charest and E. M. Vedula, *Sci. Rep.*, 2022, **12**(1), 1–14.